

## A novel nonviral gene delivery tool of BMP 2 for the reconstitution of critical size bone defects in rats

Andreas Kolk, Thomas Tischer, Christian Koch, Stephan Vogt, Bernhard Haller, Ralf Smeets, Kilian Kreutzer, Christian Plank, Oliver Bissinger

### Angaben zur Veröffentlichung / Publication details:

Kolk, Andreas, Thomas Tischer, Christian Koch, Stephan Vogt, Bernhard Haller, Ralf Smeets, Kilian Kreutzer, Christian Plank, and Oliver Bissinger. 2016. "A novel nonviral gene delivery tool of BMP 2 for the reconstitution of critical size bone defects in rats." *Journal of Biomedical Materials Research Part A* 104 (10): 2441–55.  
<https://doi.org/10.1002/jbm.a.35773>.



# A novel nonviral gene delivery tool of BMP-2 for the reconstitution of critical-size bone defects in rats

Andreas Kolk,<sup>1,2</sup> Thomas Tischer,<sup>3</sup> Christian Koch,<sup>2</sup> Stephan Vogt,<sup>3</sup> Bernhard Haller,<sup>4</sup>  
Ralf Smeets,<sup>5</sup> Kilian Kreutzer,<sup>1</sup> Christian Plank,<sup>2</sup> Oliver Bissinger<sup>1</sup>

<sup>1</sup>Department of Oral and Maxillofacial Surgery, Klinikum rechts der Isar, Technical University Munich, Ismaninger Str. 22, 81675 Munich, Germany

<sup>2</sup>Institute of Molecular Immunology and Experimental Oncology, Klinikum rechts der Isar, Technical University Munich, Ismaninger Str. 22, 81675 Munich, Germany

<sup>3</sup>Department of Orthopaedic Sports Medicine, Klinikum rechts der Isar, Technical University Munich, Ismaninger Str. 22, 81675 Munich, Germany

<sup>4</sup>Institute of Medical Statistics and Epidemiology, Klinikum rechts der Isar, Technical University Munich, Ismaninger Str. 22, 81675 Munich, Germany

<sup>5</sup>Department of Oral and Maxillofacial Surgery, University Medical Center Hamburg-Eppendorf, Martinistr. 52, Hamburg 20246, Germany

## INTRODUCTION

Bone defects following trauma or ablative surgery result in high demand for new bone (NB) to replace and restore the original shape and function of the lost osseous regions.<sup>1</sup> Although the body possesses its own capacity to heal spontaneously and to integrate metallic implants, osseous regrowth or the integration of implants is not always satisfactory, especially in the elderly population. However, in severe pathological situations, autogenous bone grafting remains one of the most common surgical procedures for

skeletal healing.<sup>2</sup> Advances in bone tissue bioengineering over the past decade have enabled the *in vivo* regeneration of living bone through the employment of various growth factors (GFs), osteogenic cells and biocompatible scaffolds or a combination of these approaches.<sup>3,4</sup> Bone morphogenetic proteins (BMPs) are the most potent osseoinductive GFs and have demonstrated a powerful ability to induce the osteogenic differentiation of mesenchymal cells as well as orthotopic and heterotopic new-bone formation and to enable bone formation in defects that would otherwise require

**Author contributions:** Authors' roles: Study design: AK and CP. Study conduct: AK and minor parts CK, SV and OB. Data collection: TT and OB. Data analysis: AK, TT, KK and OB. Data interpretation: AK, CP, BH and OB. Drafting manuscript: AK and CP. Revising manuscript content: AK, CP and OB. Approving final version of manuscript: AK, TT, SV, KK, RS, OB. AK and CP take responsibility for the integrity of the data analysis.

**Correspondence to:** A. Kolk; e-mail: andreas.kolk@tum.de

Contract grant sponsor: German Federal Ministry of Education and Research Grand; contract grant number: BMBF 0312019A

Contract grant sponsor: Nanosystems Initiative Munich (NIM)

autogenous bone tissue transfer for repair.<sup>5,6</sup> However, GFs also present several disadvantages, such as short half-lives, high costs, potential systemic side effects, an incompletely understood dose dependency, tissue selectivity and potential inactivation through, for example, interference with other systemic GFs.<sup>7</sup> In addition, it is difficult to achieve spatial and temporal control of their bioactivity. The lack of controlled delivery systems is one of the reasons that excessive, cost-intensive dosages in the milligram range are required in current clinical practice.

As an alternative, gene therapy (GT)-based approaches are well established in preclinical studies for the induction of tissue regeneration, and numerous tissue defect models for bone and cartilage regeneration have been described.<sup>8-13</sup> In these approaches, a gene vector (GV) that contains the GF gene of interest is locally applied to the tissue defect, often in combination with a biomaterial matrix or autologous cells. Consequently, the resident host or transplanted cells will locally express the GF of interest in the tissue defect when transduced/transfected with the GV. BMP transgenes have often been used for bone repair, and successful results have been reported in various animal experiments.<sup>2,11,13</sup> Regional GT can be exploited for the short- or long-term expression of osteogenic cytokines to stimulate osteogenesis.<sup>2,9</sup>

Sustained expression, as a consequence of sustained localized vector release and uptake in resident cells, can be achieved through the gene-activated matrix (GAM) concept, that is, a GV embedded in a biomaterial matrix.<sup>11,14</sup> In addition, inducible promoters can control transgene expression. Hence, the GAM concept allows for the implementation of the spatio-temporal control of GF bioactivity.<sup>15</sup> Although various systems have been applied to promote gene delivery *in vivo*, the contribution of the release rate to gene expression *in vivo* has not been well defined, particularly in the context of plasmid design, expression silencing, safety and dose dependency.<sup>2,14,16,17</sup> The variety of gene dosages, carrier systems and materials used along with the lack of continuous release data make a comparison of study data and the forecasting of optimal dosages difficult. In a previous *in vitro* study, we demonstrated a specific predictable dose dependency of a nanoparticle-based nonviral GV system for the GF BMP-2.<sup>18</sup> BMP-2 was chosen for comparison with previous *in vitro* data and because, apart from BMP-7, it is the only GF approved by the Food and Drug Administration (FDA) for clinical use to promote bone regeneration.<sup>19,20</sup> In the present animal experiment, this method of gene delivery from a stable, coated metallic surface was modified to maximize its osteogenic potential. The goals were to evaluate the transferability of the previously published *in vitro* data to an *in vivo* model. Therefore, a series of different concentrations of pBMP-2 was employed to investigate the dose dependency, time course and localisation of NB formation within critical-size defects (CSDs). We hypothesized that the incorporation of the BMP-2 plasmid into a stable poly(D, L-lactide) (PDLLA) coating would give rise to an enhanced effect on bone healing. Rats were chosen as the preferred animal's model due to similar receptors of bone cells, osteo-

blasts, osteocytes, and osteoclasts compared to human bone cells. Reaction to drug challenge can be expected analogous to human bone.

## MATERIALS AND METHODS

### Materials

If not stated otherwise, reagents were purchased from Sigma-Aldrich (Taufkirchen/Munich, Germany). Titanium foils of 20  $\mu\text{m}$  in thickness were purchased from Friadent, Mannheim, Germany. Discs of 8 mm in diameter were punched from the foil using a die cutter. The 25-kDa branched polyethylenimine (PEI) used in this study was prepared as an aqueous stock solution neutralized with hydrochloric acid. PDLLA, namely, Resomer 203 (inherent viscosity: 1.8  $\text{dL g}^{-1}$ , molecular weight: 30 kDa), was purchased from Boehringer Ingelheim (Ingelheim, Germany). All vector components (plasmid DNA, PEI, and protective copolymer) were stored as stock solutions in deionised water. The plasmid p55pCMV-IVS-luc+, which codes for firefly luciferase as a reporter gene under the control of the CMV promoter, was kindly provided by Andrew Baker (Bayer). The plasmid pBMP-2 was derived from p55pCMVIVS-luc+ by removing the luciferase-encoding sequence using the Qiagen (Hilden, Germany) gel extraction kit after Hind III/Fse I digestion and by inserting the BMP-2-coding sequence, which was amplified by the polymerase chain reaction (PCR), to introduce Hind III/Fse I restriction sites. The plasmids were expanded and purified using chromatographic techniques by Plasmid Factory GmbH & Co. KG (Bielefeld, Germany).

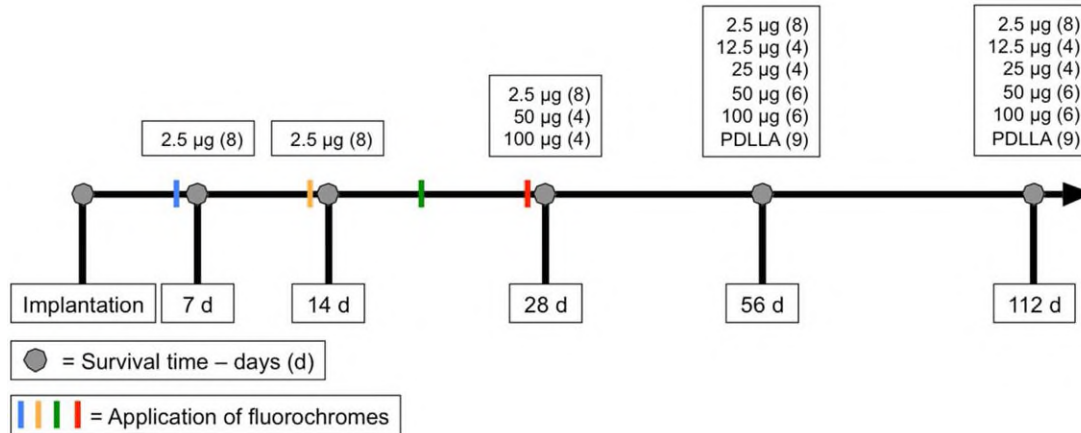
### Copolymer-protected gene vectors (COPROGS)

The copolymer-protected gene vectors (COPROGS) and PDLLA-coated titanium discs used in this study were prepared as described previously.<sup>18</sup> Briefly, COPROGS were prepared in water from 25-kDa branched PEI and plasmid DNA at an *N/P* ratio of 8 and were coated with a layer of the negatively charged protective copolymer P6YE5C. The latter was synthesised as described by Finsinger et al.<sup>21</sup> with slight modifications as described recently.<sup>8,18,22</sup> The complexes were lyophilised, and the resulting powder was homogeneously resuspended in 50 mg/ml PDLLA solutions in ethyl acetate using a Teflon® pestle (Schütt Labortechnik, Göttingen, Germany) at the desired vector concentration.

### Implant fabrication

Granular powder of amorphous PDLLA was dissolved in ethyl acetate at a concentration of 50 mg/ml. Lyophilised COPROGS that contained the plasmid of interest (p55pCMV-IVS-luc+ or pB-BMP-2) were dispersed in this solution at the desired COPROG concentrations of 0, 2.5, 12.5, 25, 50, and 100  $\mu\text{g}$  plasmid per 25  $\mu\text{L}$  PDLLA solution using a Teflon® pestle. *In vitro* concentration lower than 2.5  $\mu\text{g}$  (for example, 1/0.5  $\mu\text{g}$ ) have proven to be ineffective in various cell lines because a significant proportion of the plasmid will remain in the coating for a long time so that in the initial 14 days of delivery only minimal concentrations of active plasmid were available for local bmp-2 expression.

**TABLE I. Timeline, Study Setup, and Time Points for Fluorochrome Application and Euthanasia, Indicating the Corresponding Numbers of Jaws/Group**



The study was initially performed using all groups at the time points of 56 and 112 days and was then performed using only the groups treated with 2.5, 50, and 100 µg pBMP-2 at day 28. Because the 2.5 µg pBMP-2 group demonstrated the best results, further testing at days 7 and 14 was conducted only for this group.

The ratio for choose of the range of tested dosage was analog to the respective *in vitro* tests, that gave us the underlying spatiotemporal information. In addition we orientated on previous own data and other lab groups using growth factor concentration of 50 µg and higher showing a mild osteopromoting effect. Aliquots of 25 µL of these dispersions were carefully applied to the titanium discs using a micropipette, resulting in a film of 1.25 mg PDLLA per implant (24.9 µg/mm<sup>2</sup>). The discs were placed in a laminar flow hood for evaporation of the solvent, followed by drying under high vacuum.

Scanning electron microscopy (SEM) images indicated a smooth, gap-free transition between the PDLLA coating and the titanium support at the boundary of the coating.

#### Animals and anaesthesia

All animal procedures were approved by the local animal research committee, in accordance with German legislative requirements, and were performed at the Centre for Preclinical Research at the Technical University of Munich (reference number: 55.2-1-54-2531-100/03). Fifty-three 6-month-old male Sprague Dawley (SD) rats (weight range: 450–500 g) were obtained from Charles River WIGA (Germany). In accordance with the standards for animal housing, the rats were single-fed, housed at 23–25°C with a 12-h light/dark cycle and allowed free access to water and standard laboratory pellets.

For lesion induction, the rats were anaesthetised with Medetomidine (Medetomin, Dechra Veterinary Products, 1.0 mg mL, Dechra Veterinary Products, 's-Hertogenbosch, Netherlands), Midazolam (Midazolam, 5 mg mL, Hexal AG, Germany) and Fentanyl (Fentadon, Dechra Veterinary Products, 50 µg mL) via body weight adapted intramuscular (i.m.) injection.

To end the anaesthesia, a body weight adapted subcutaneous injection of an antidote combination was given, com-

posed of Atipamezole (Antisedan, 5 mg/mL, Orion Corporation, Espoo, Finland), Flumazenil (Flumazenil, 0.1 mg mL, Hexal AG), and Naloxone hydrochloride (Naloxone, 0.4 mg/mL, Braun AG, Germany)

During the first week after surgery, the animals were administered subcutaneous injections of buprenorphine twice a day (Buprenodale, 0.3 mg/mL, Dechra Veterinary Products) for pain relief.

#### Study design

In each group, all animals ( $n = 53$ ) bilaterally received one of the coated titanium implants. The mandibular defects were randomly divided into six groups (A–F) and covered with the following amounts of pBMP-2/implant: (A) 2.5 µg ( $n = 40$ ); (B) 12.5 µg ( $n = 8$ ); (C) 25 µg ( $n = 8$ ); (D) 50 µg ( $n = 16$ ); (E) 100 µg ( $n = 16$ ); and (F) PDLLA alone ( $n = 18$ ) (Table I). The study began with the testing of all of the groups, A–F, at time points of 56 and 112 days, and additional testing was then performed for groups A, D and E at day 28 and for group A at days 7 and 14. Following qualitative and quantitative evaluation of the results using various methods of analysis, group A was identified as superior to all other groups. To avoid unnecessary loss of animal lives, in accordance with the 3-R principle (replacement, refinement, and reduction), the remainder of the studies and time-point analyses were conducted using the 2.5 µg pBMP-2 group only. The time points in this study were chosen to cover the maximum time span of bone turnover based on the time courses of mandibular bone defect healing observed in previous experiments.<sup>23,24</sup>

#### Surgical procedure

Using a standard round trephine bur (Friadent, Mannheim, Germany), transosseous defects of 5 mm in diameter were drilled bilaterally in 53 rats as already described.<sup>25</sup> Because of the 8-mm diameter, the implants extended ~1.5 mm

outside the margins of the defect. They were tightly adapted to the surrounding bone and fixed by the repositioned periosteum and masseter muscle. Subsequently, the soft tissues and skin were carefully redraped and closed in layers using 4–0 resorbable sutures.

Before the rats were sacrificed at the end of the experiment on the respective day via an overdose of Narcoren (sodium pentobarbital, 80 mg/kg bw), they were anaesthetised in a plastic box via inhalation of isoflurane.

### Radiographic analysis and micro-CT measurements

All mandibles were dissected free of soft tissue, fixed in 100% methanol and stored at 4°C (overnight) until micro-CT ( $\mu$ CT) scanning was performed. Prior to  $\mu$ CT measurement, X-ray images of the mandibles were acquired using a dental X-ray machine (Gendex Corporation, Des Plaines, IL) from a distance of 7 cm (70 kV, 7 mA) with an exposure time of 0.08 s. A small X-ray tube was used as the source.

To evaluate NB formation, all mandibles were then scanned via  $\mu$ CT at an isotropic voxel size of 10  $\mu$ m (55 kVp, 145  $\mu$ A;  $\mu$ CT 40, Scanco Medical, Brüttisellen, Switzerland).<sup>26–28</sup> For each sample,  $\sim$ 302  $\mu$ -tomographic slices (depending on the amount of bone regeneration) were acquired with a slice increment of 8  $\mu$ m, covering the entire medial-lateral width of the defect ( $\sim$ 4.53 mm). From these two-dimensional (2D) images, a volume of interest (VOI) of 5 mm in diameter was determined<sup>29,30</sup> and three-dimensional (3D) CT images were reconstructed.<sup>27,29</sup>

The following measures of bone structure and composition were evaluated based on the  $\mu$ CT image data for each specimen: mineralised callus volume (BV, mm<sup>3</sup>), tissue mineral density (TMD, mg HA/cm<sup>3</sup>) and bone mineral content (BMC, defined as the callus BV multiplied by the TMD, mg).<sup>26,30</sup>

To confirm the effects of locally available stem/progenitor cells and vascular supply on BV, we further divided the 2.5  $\mu$ g pBMP-2 group into two subgroups based on the distance from the CSD to the root of the mandibular incisor of the rat (Fig. 1).

To analyze the pattern of bone regeneration throughout each entire CSD, we divided the CSD into nine fields using a grid template (Fig. 1). Each single field was then further analyzed to determine the amount of NB. For this purpose, we awarded 1 point for completely consolidated fields, whereas empty squares without any bone growth were evaluated as 0 (V 1–3, M 1–3, D 1–3). Thus, regenerated squares could be contrasted with unconsolidated fields. To simplify the analysis, we formed two fractions, ventral (V 1–3 + M 1) and dorsal (M 2 + 3 + D 1–3) (Fig. 1).

### Histological and histomorphometric analysis

After  $\mu$ CT analysis, the specimens ( $n = 53$ ) were dehydrated in a graded series of ethanol (from 70% to 100% [v/v]) and acetone and were then embedded in methyl methacrylate (MMA).

After polymerisation, sections of the MMA-embedded samples of  $100 \pm 10$   $\mu$ m in thickness were prepared using a sawing microtome (Leitz, Wetzlar, Germany) technique as

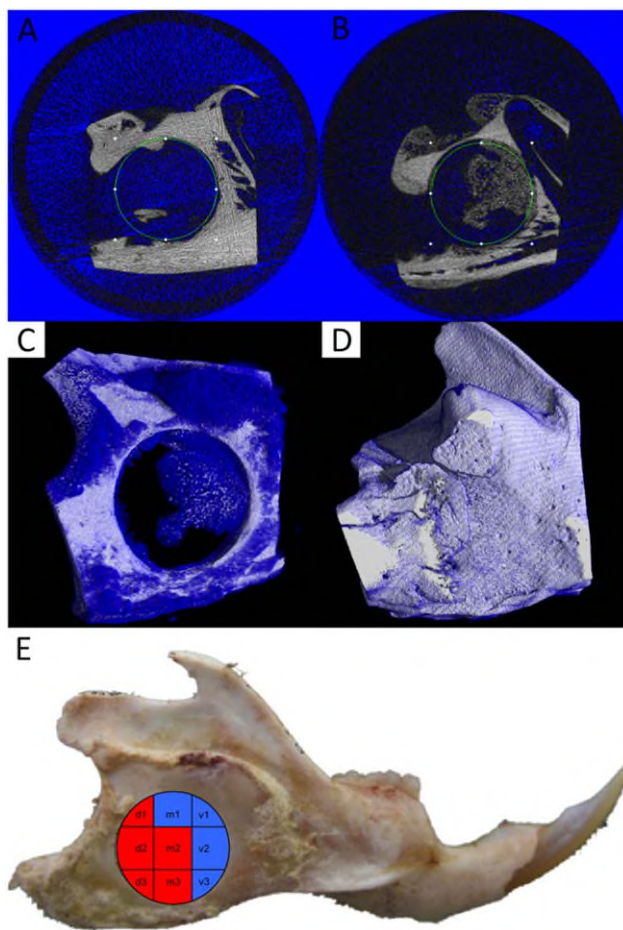


**FIGURE 1.** Two-dimensional (A and B) and three-dimensional (C and D)  $\mu$ CT images of the CSD region: Division of the 2.5  $\mu$ g pBMP-2 group into two subgroups: (A) not adjacent to the periodontal ligaments and (B) in direct contact with the incisor root. Color-coded illustration of the difference between the newly formed woven bone after 14 days (C, dark blue color-coded NB; corresponding to image B) and the well-organised lamellar bone observed after 112 days (D, the entire former defect appears in the same light blue color as the adjacent original bone). (E) Nine-field division of each CSD for the evaluation of the localisation of the NB within the defect. Mandible and grid template illustrating the simplification of the analysis through the formation of two fractions, ventral (V 1–3 + M 1) and dorsal (M 2 + 3 + D 1–3).

described by Donath and Breuner.<sup>31</sup> A series of 13–14 sections was cut coronally through each sample. Select specimens were additionally ground (70  $\mu$ m) and polished (Schleifsystem 400 CS, Exakt, Germany). For histological analysis, the sections were surface stained as described by Laczkó and Lévai (LL),<sup>32</sup> and analysis was performed via bright-field microscopy (Axiophot 2; Zeiss, Jena, Germany). A video camera (AxioCam MRC 5, Zeiss, Jena, Germany) interfaced with a workstation was used to project images onto a monitor. Quantitative analysis was performed using an image analysis system (Kontron KS 400 image analysing system; Zeiss, Jena, Germany), as previously explained.<sup>33</sup> The staining afforded sufficient dyeing contrast to distinguish NB from mature bone (dark red), from osteoid (light red) and from fibrous tissue/cartilage (blue).<sup>34,35</sup> Furthermore, the

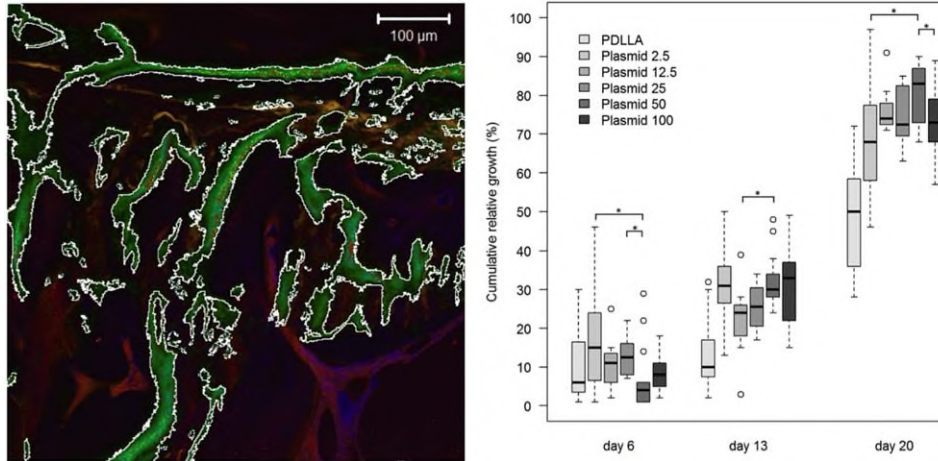


**FIGURE 2.** (Left) Overlay illustration of the semi-automatic surface measurement of calcein-green-labelled bone in the ROI. Scale bar = 100  $\mu\text{m}$ . (Right) Fluorochrome labelling of the NB: differences in the cumulative bone-inducing activity among the different groups derived from the time of FL application on day 6, 13, and 20. Adding up to 100% on day 27 this data are not displayed. Calcein, a FL administered during the second postoperative period, was the most extensively marked label. A significant difference in the share of bone-inducing activity ( $p < 0.05$ ) was seen between the experimental groups (\*). Concerning the PDLLA control group, no significant difference could be seen on day 6, but as expected there was significant less bone-inducing activity ( $p < 0.05$ ) on day 13 and 20 compared to all therapy groups. For clarity this is not displayed in the figure. (Time points refer to the day of FL application).

sections were dyed with Goldner's Masson trichrome (TMG)<sup>36</sup> and Von Kossa's staining (vK) that selectively reveal mineralised structures of NB at a diffusion depth of 1 mm.<sup>37</sup>

For quantitative histomorphometric comparison among the groups, the completely mineralised and immature bone volume (with areas of fibrous tissue subtracted) was evaluated by obtaining a 2D measurement (distance and area). First, the total area of the former CSD was calculated, and then, the total extent of NB growth within the CSD was measured and subtracted from this total area. Subsequently, the 2D transverse sections of NB were combined within the CSD, resulting in a 3D form for correlation with the  $\mu\text{CT}$  data.

### Microradiography

The nondecalcified resin-embedded central sections from each jaw ( $n = 106$ ) were reduced to 100–120  $\mu\text{m}$  using a grinding unit (Exakt Apparatebau GmbH, Norderstedt). Contact microradiography was performed on high-resolution photographic plates (IMTEC, Sunnyvale, Calif., USA) using a Faxitron Microfocus System (Hewlett-Packard; Palo Alto, CA, USA) with a period of exposure of 50 min at 25 kV and 2.5 mA.

The developed X-rays (Kodak, Stuttgart, Germany) were scanned using an Epson scanner at 1200 dpi and 12-bit greyscale and were stored in TIFF format. The mineralisation ratios in the defect area in all groups for days 14, 28, 56, and 112 were analyzed using Bioquant Osteo software V7.10.10 (BIOQUANT Image Analysis Corporation, Nashville, TN).

### Polychrome labelling of bone

In accordance with the general principles described by Rahn et al.,<sup>38,39</sup> polychrome sequential fluorescent labelling (FL) was performed in a modified manner using an extended number of fluorochromes to mark the mineralised

tissue and to assess the time course of the initial NB formation and early mineralisation process, as previously described by the authors.<sup>40,41</sup> To quantify the latter, we chose early time points for FL in contrast to the  $\mu\text{CT}$  imaging. Four different fluorochromes were subcutaneously administered to all animals with a survival time of at least 28 days under intramuscular anaesthesia with 250 mg Zolazepam and 250 mg Tiletamine (Tilet 500, Parke-Davis, Freiburg, Germany). FL was initiated at day 6 after the surgical procedure and continued for 3 weeks with one injection per week as follows: day 6, calcein blue (30 mg/kg calcein blue; Sigma, USA); day 13, xylenol orange (90 mg/kg xylenol orange tetrasodium salt; Sigma, USA); day 20, calcein green (15 mg/kg calcein; Sigma, USA); and day 27, alizarin complexone (30 mg/kg alizarin red S; AL, Sigma, USA). Quantitative analysis was performed on 80- $\mu\text{m}$ -thick unstained coronal sections using a confocal laser scanning microscope (CLSM 510 META NLO, Carl Zeiss, Germany). The amount of fluorescently labelled bone within the CSD was measured ( $\mu\text{m}^2$ ) for two regions of interest (ROI) in each specimen. The image stack was subdivided into the various fluorochromes, representing the percentage of calcification like the bone turn over at each specific time point, via automatic component extraction. Image acquisition and post-processing were performed using AIM software (Carl Zeiss, Germany); semi-automatic measurements were performed using the ImageJ freeware package provided online by the NIH (U.S. National Institutes of Health) (Fig. 2).

### Statistical analysis

All presented data were obtained from the analysis of the bone specimens and are presented as the means  $\pm$  standard deviations. To address the question of whether the time

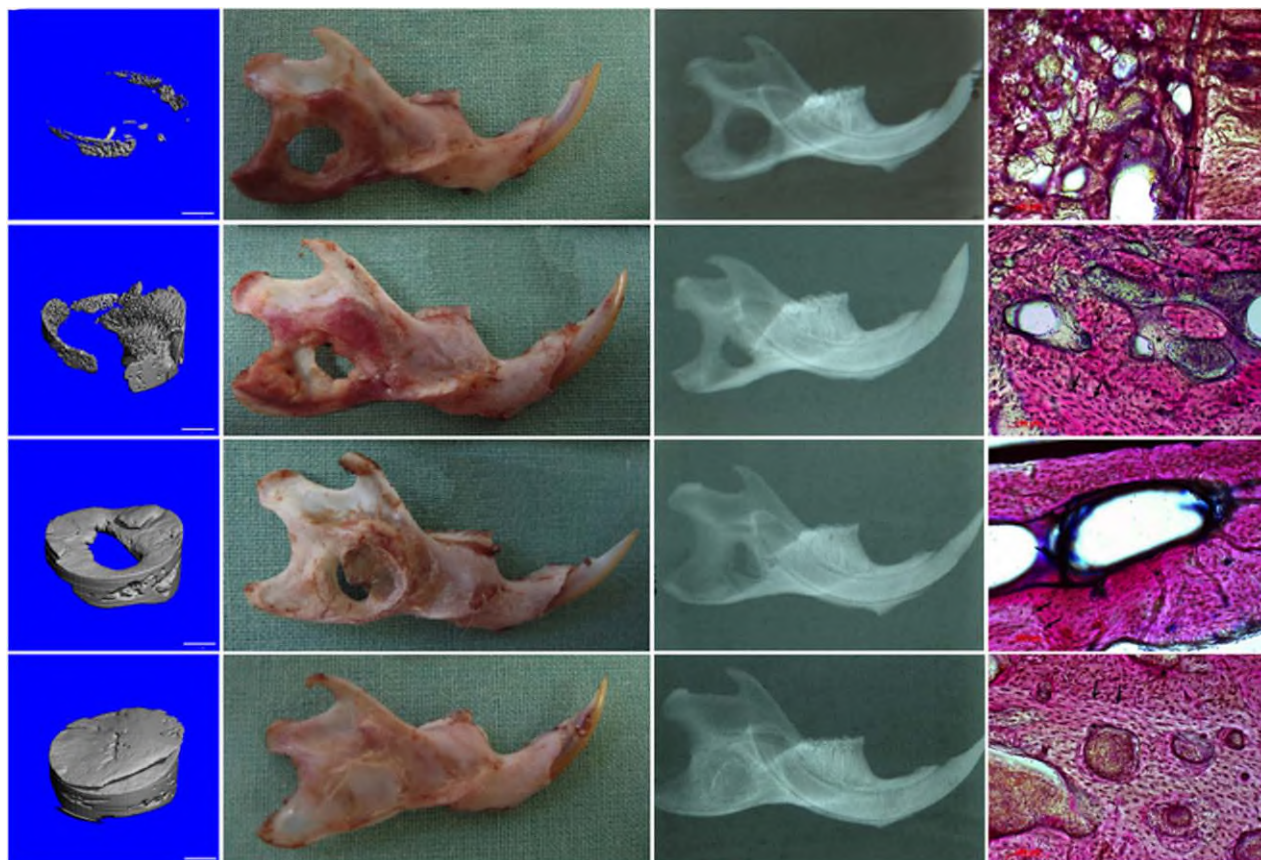


**FIGURE 3.**  $\mu$ CT (scale bar = 1 mm), clinical, radiographic (dental X-ray) and histological evaluations of the course of bone ingrowth within the CSDs (2.5  $\mu$ g pBMP-2-transfected group, days 14, 28, 56, and 112, from top to bottom). The various representative images or photographs reveal well-defined radio-opacities within the CSD; these were completely regenerated after 112 days. Histology (scale bar = 100  $\mu$ m) reveals the transition zone between the NB and the original bone (arrows), and asterisks indicate the osteoid trabeculae (100x magnification).

point, the plasmid concentration and the localisation of the CSD with respect to the incisor root exerted any influence on the resulting NB formation, comparisons were performed using the unpaired two-tailed Student's *t* test. To differentiate squares (paired conditions) within the nine-field division of the CSD, the fields were summed into two larger regions (ventral and dorsal), and comparisons of ossification between the two were performed using the McNemar test. The association between the  $\mu$ CT and histomorphometry results was evaluated using the Spearman's rank correlation coefficient test. A level of significance of  $\alpha = 5\%$  was set for all tests. All statistical analyses were performed using the IBM

SPSS statistics software package (Version 18; SPSS, Chicago, IL) and R version 2.15.2 (R Core Team (2013), Vienna, Austria).

## RESULTS

All animals survived the surgical procedures, and with the exception of two from the 25  $\mu$ g pBMP-2 group (death after 4/5 days), all were available for evaluation. All surgical interventions healed well. No implant was lost. Upon palpation during the retrieval of bone specimens, all titanium implants appeared to be firmly fixed in the original region of application. At 10–14 days after implantation, peri- and

**TABLE II.** Data from  $\mu$ CT Measurements of Bone Volume (BV,  $\text{mm}^3$ ) Within the Former CSDs Over Time (days 7–112)

Group	7 days	14 days	28 days	56 days	112 days
A 2.5	2.24 $\pm$ 2.85	4.21 $\pm$ 2.18	7.07 $\pm$ 3.95	6.99 $\pm$ 4.19	12.57* $\pm$ 4.67
B 12.5				5.10 $\pm$ 2.48	5.85 $\pm$ 2.92
C 25				8.08 $\pm$ 5.59	10.33 $\pm$ 4.45
D 50			1.63 $\pm$ 1.62	2.64 $\pm$ 1.82	1.88 $\pm$ 1.07
E 100			1.24 $\pm$ 0.84	2.51 $\pm$ 1.90	3.67 $\pm$ 3.13
F PDLLA				8.69 $\pm$ 2.69	5.64 $\pm$ 4.97

The 2.5  $\mu$ g pBMP-2 group exhibited continuous enhancement in BV from 2.24  $\pm$  2.85  $\text{mm}^3$  to 12.57  $\pm$  4.67  $\text{mm}^3$ . Entries marked with \* represent significant differences relative to the previous time point (\* $p < 0.05$ , \*\* $p < 0.01$ , \*\*\* $p < 0.001$ ), for significances between groups see Figure 4.

**TABLE III. Data from  $\mu$ CT Measurements of Tissue Mineral Density (TMD, mg HA cm<sup>3</sup>) Within the Former CSDs Over Time (Days 7–112)**

Group	7 days	14 days	28 days	56 days	112 days
A 2.5	825.00 ± 91.67	742.55 ± 85.68	848.01* ± 57.83	913.92* ± 29.22	1051.42*** ± 29.73
B 12.5				955.68 ± 25.07	1015.32* ± 25.49
C 25				985.79 ± 79.78	1022.16 ± 23.79
D 50			787.50 ± 14.46	909.74 ± 85.95	1024.43* ± 35.18
E 100			848.86 ± 17.68	922.41* ± 34.10	996.02** ± 35.28
F PDLLA				936.04 ± 45.22	1014.94** ± 35.45

With the exception of the 25  $\mu$ g pBMP-2 group, the observed differences in TMD over time were more significant than those in BV for all groups (2.5, 12.5, 50, 100  $\mu$ g pBMP-2 and native PDLLA). Entries marked with \* represent significant differences relative to the previous time point (\* $p < 0.05$ , \*\* $p < 0.01$ , \*\*\* $p < 0.001$ ).

submandibular seromas occurred in the 50 and 100  $\mu$ g pBMP-2 groups (high COPROG dosages).

### Quantitative and qualitative assessment of newly formed bone

To evaluate a plane overview of the NB-formation, dental X-ray images were acquired in the former defect region at 14–112 days after surgery to create the CSD. Representative photographs of the 2.5  $\mu$ g pBMP-2 group are presented in Figure 3. Radio-opacities indicating a lack of bone regeneration within the defect sites were detected in the following groups: native PDLLA and 100, 50, 25, and 12.5  $\mu$ g pDNA. In contrast, a considerable increase in bone growth was observed in the samples covered with 2.5  $\mu$ g-plasmid-coated implants after 56 and 112 days (Fig. 3). Although NB formation was also observed in the native PDLLA group, this formation was stronger at the anterior edge of the defect rather than being homogeneously distributed over the entire defect, as was the case in the 2.5  $\mu$ g pBMP-2 group.

The  $\mu$ CT technique was used to evaluate the microstructural morphology of the NB and to measure the spatio-temporal differences in the BV and TMD parameters between the treatment and control groups.

With respect to the time course, the best-performing group with 2.5  $\mu$ g pBMP-2 exhibited a continuous enhancement in BV over time (days 7–112), from  $2.24 \pm 2.85 \text{ mm}^3$  to  $12.57 \pm 4.67 \text{ mm}^3$  ( $p < 0.05$ , Table II). In contrast, the BV of the PDLLA-induced bone notably declined between the 56th and 112th days.

With the exception of the 25  $\mu$ g pBMP-2 group, the differences in TMD over time were more significant than those in BV for all groups ( $p < 0.001$ – $0.05$ , Table III). This result can be visualised from a colour-coded representation of the density based on the brightness distribution of the voxel. The brighter shades of blue represent the increase in density over time (Fig. 1).

With respect to the dose dependency, the defects treated with 50 or 100  $\mu$ g pBMP-2 failed to exhibit any positive effects on bone regeneration; only a minor region of the defects was covered (that is, an inverse dose–response relationship was observed) (Fig. 4). With decreasing concentration, an increasing volume was observed, leading to complete consolidation (Figs. 3 and 4) at a concentration of 2.5  $\mu$ g. Significant differences in BV were observed between the

groups treated with 2.5–25  $\mu$ g pBMP-2 and the groups treated with 50–100  $\mu$ g pBMP-2 at days 56 and 112 ( $p < 0.05$ , Fig. 4). Representative  $\mu$ CT scans of each group at 56 and 112 days are presented in Figure 4.

In addition to the abovementioned dose effects, the 2.5  $\mu$ g pBMP-2 group also exhibited significant differences in TMD (most similar to native bone:  $1138.64 \pm 26.62 \text{ mg HA cm}^{-3}$ ) at the final time point of 112 days compared with the high-concentration group of 100  $\mu$ g pBMP-2 and the control group (native PDLLA) ( $p < 0.05$ ) (Fig. 4).

Regarding the bone mass, no new behavior was observed that was not already evident from the BV.

The organic spread of luciferase (group G, subsumed into group F for evaluation of BV) could be excluded via PCR (data not shown), as in a previous study using the same vector and coating technology.<sup>42</sup>

The effect of the localisation of the CSD with respect to the root of the mandibular incisor of the rat was then analyzed. The subgroup of the 2.5  $\mu$ g pBMP-2 group in which the CSD was in direct contact with the incisor root exhibited significantly more NB formation than did the other subgroup, in which the CSD was not adjacent to the periodontal ligaments [ $8.26 \pm 4.91 \text{ mm}^3$  to  $5.39 \pm 3.49 \text{ mm}^3$ ,  $p < 0.05$ , Fig. 1(A,B)]. The pattern of bone regeneration within the defect is illustrated in Figure 5. Thus, we observed that the regeneration within the ventral fraction (V 1–3 + M 1) was significantly superior to that in the dorsal fraction (M 2 + 3 + D 1–3) in the groups treated with 2.5 and 12.5  $\mu$ g pBMP-2.

### Histological examination and histomorphological analysis

The objective of the histomorphological analysis was to chronologically evaluate the formation and maturation processes of bone ingrowth within the CSD as a function of the applied concentration of COPROGs.

No evidence of a local inflammatory response to the therapy was detectable in any group. After 14 days of regeneration with 2.5  $\mu$ g pBMP-2, a predominance of woven immature bone was surrounded by distinct layers of unmineralised osteoid, fibrous cells and some empty osteocytic lagoons, especially on the ventral side of the CSD, separating the NB from the original local bone. The immature bone exhibited more intense staining, with various colors depending on the stain used (Fig. 6), than did the remodelled lamellar-like bone

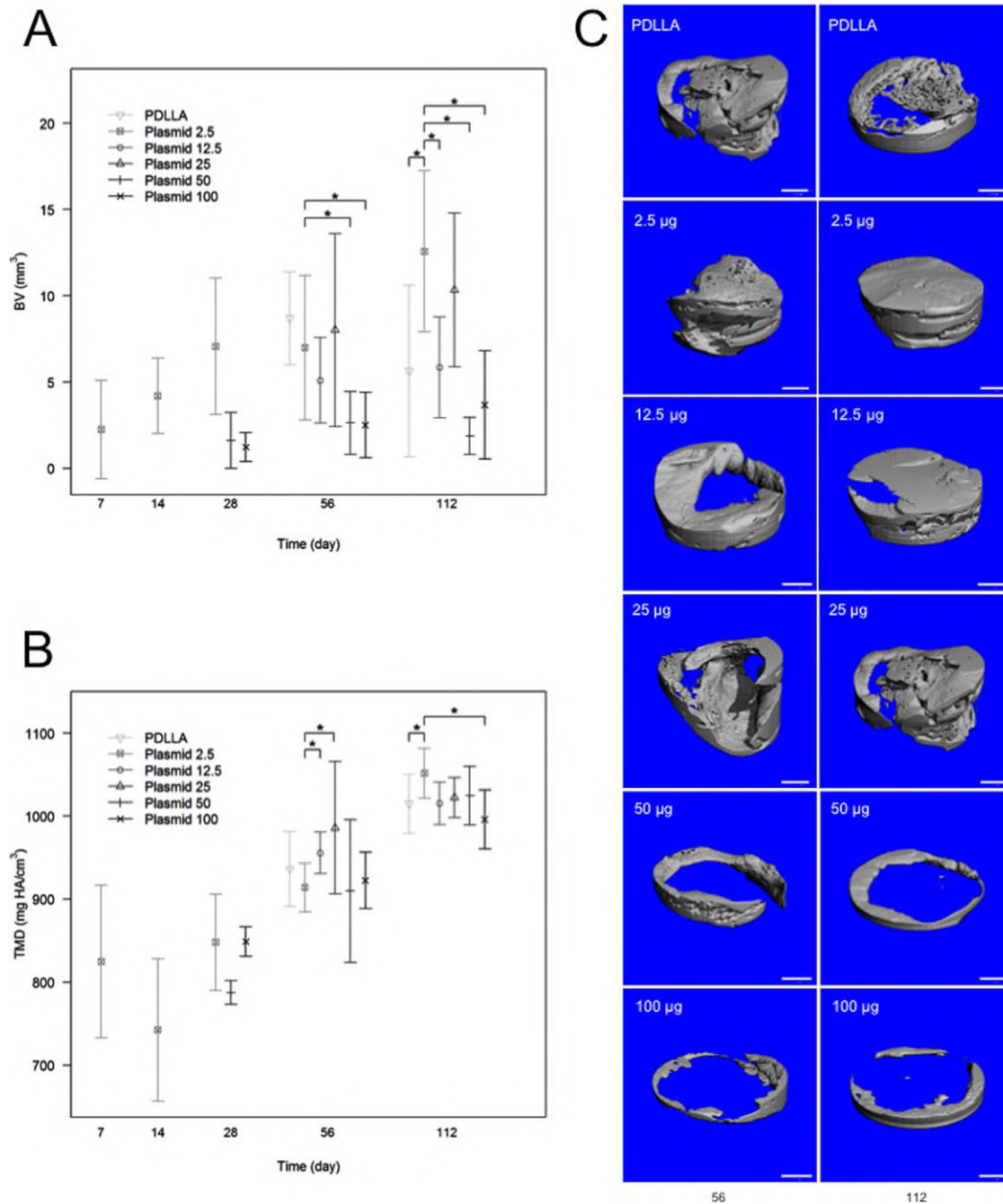


**FIGURE 4.**  $\mu$ CT measurements of the dose-dependent (A) BV and (B) TMD values of all plasmid groups at the corresponding time points. Significantly higher BV values were observed in the 2.5  $\mu$ g pBMP-2 group compared with the groups treated with 50 and 100  $\mu$ g pBMP-2 at day 56 and compared with the groups treated with 12.5, 50, and 100  $\mu$ g pBMP-2 and native PDLLA at day 112, and significant higher TMD values were observed in the 2.5  $\mu$ g pBMP-2 group compared with the groups treated with 12.5 and 25  $\mu$ g pBMP-2 at day 56 and compared with the groups treated with 100  $\mu$ g pBMP-2 and PDLLA at day 112. The data represent the means  $\pm$  SDs, and the notation \* indicates significance at  $p < 0.05$  from the 2.5  $\mu$ g pBMP-2 group at the specific time point with respect to all other groups. Other significances are not shown. (C) 3D reconstructions of NB formation in the VOI after 56 (left) and 112 (right) days in ascending order of pBMP-2 concentration and PDLLA, from top to bottom: PDLLA, 2.5, 12.5, 25, 50, and 100  $\mu$ g. There is a visible inverse dose dependency, with minimal NB formation in the contact area between the implant and the edge of the CSD in the 50 and 100  $\mu$ g groups but an increasing trend in BV with decreasing concentration, culminating in full consolidation for treatment with 2.5  $\mu$ g. Scale bar = 1 mm.

tissue or the pre-existing mature bone (Fig. 7). The latter could also be confirmed via 3D color-coded  $\mu$ CT imaging, which revealed clear differences in density between the NB and the pre-existing bone (Fig. 1).

Following 28 days, compared with day 14, a relevant proportion of parallel-fibred woven bone appeared predominantly in the ventral region of the CSD, with a slight decrease in immature areas. Fibrous connective tissue

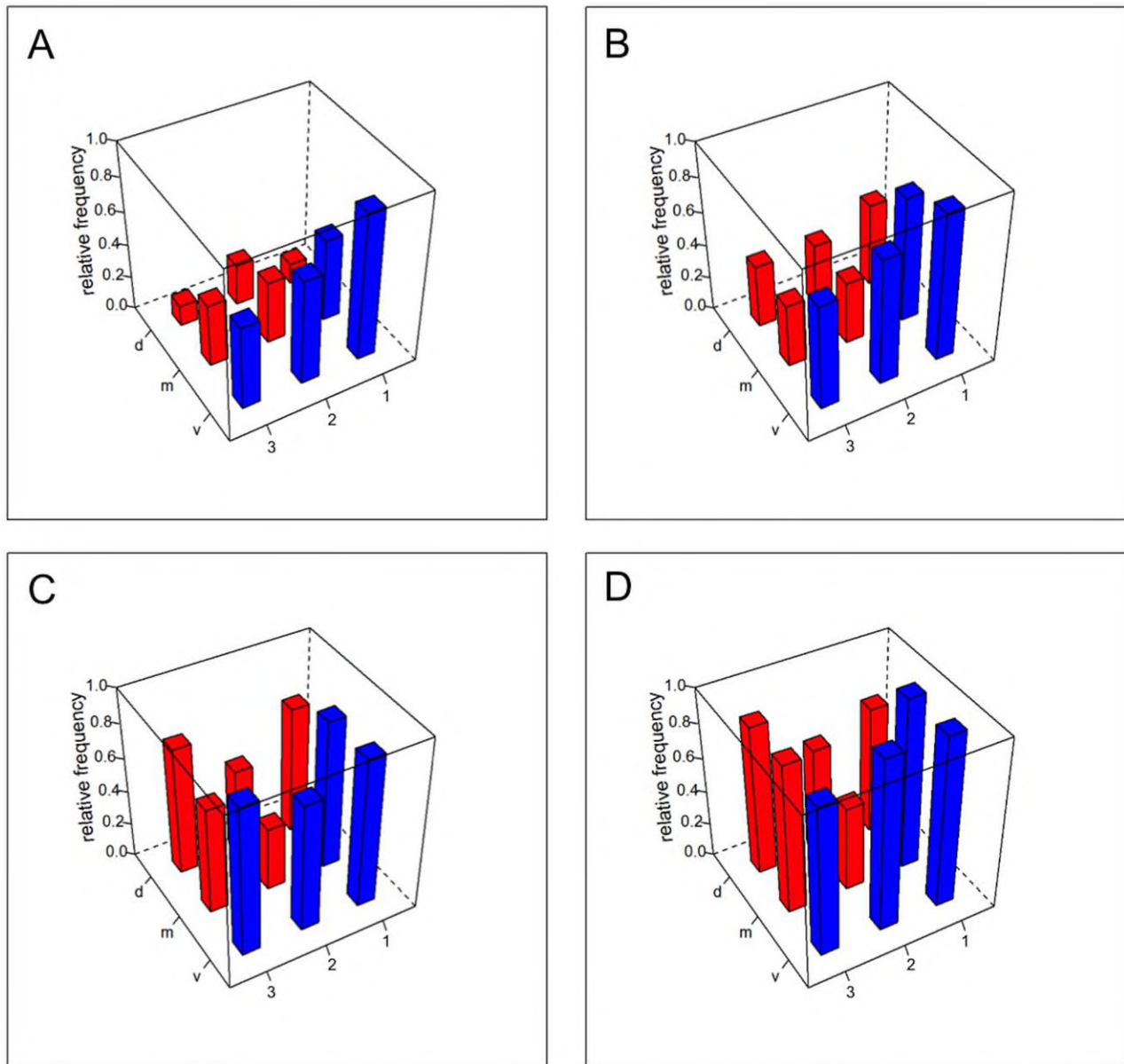


**FIGURE 5.** Example of field-dependent bone ingrowth over time in the 2.5  $\mu\text{g}$  group at days (A) 14, (B) 28, (C) 56, and (D) 112. The regeneration in the ventral fraction (V 1-3 + M 1) was significantly superior to that in the dorsal fraction (M 2 + 3 + D 1-3) at all time points (day 56,  $p < 0.05$ ; days 14, 28, and 112,  $p < 0.01$ ).

was minimally present in only the distal region of the defect. Within these regions, TMG (Fig. 6) revealed the presence of both immature (osteoid) and mature bone and portions of osteoblasts embedded within an osteoid matrix located on the growth front adjacent to the edge of the defect. At the cellular level, osteocytes could be differentiated from osteoblasts primarily at the transition from the NB to the local pre-existing bone edge of the CSD. Additionally, sporadic osteoclasts were visible under TMG and LL staining.

At time point 56 days, more areas with organised lamellar bone, with characteristics increasingly similar to those of the pre-existing local bone, were observed. Compared with previous time points, the transition from the clear osteocyte

structures of the original bone to the osteoid and matrix formed by the osteoblasts was no longer as apparent. Similarly, the connective tissue formerly lying between and formed of elastic and reticular fibres and fibroblasts was less obvious.

Consistent with the findings obtained via  $\mu\text{CT}$ , the treatment with 2.5  $\mu\text{g}$  pBMP-2 led to the greatest amount of ossification, with histological evidence of the complete filling of the CSD after 112 days. Mature, newly formed bone tissue without fibrous connective tissue was evident. At higher magnification, the lamellar structures of the ossified bone tissue had a healthy appearance, as indicated by the thickness of the well-organised lamellar bone. The lines of cementation exhibited smooth, straight contours (Fig. 7). PDLLA revealed a partial

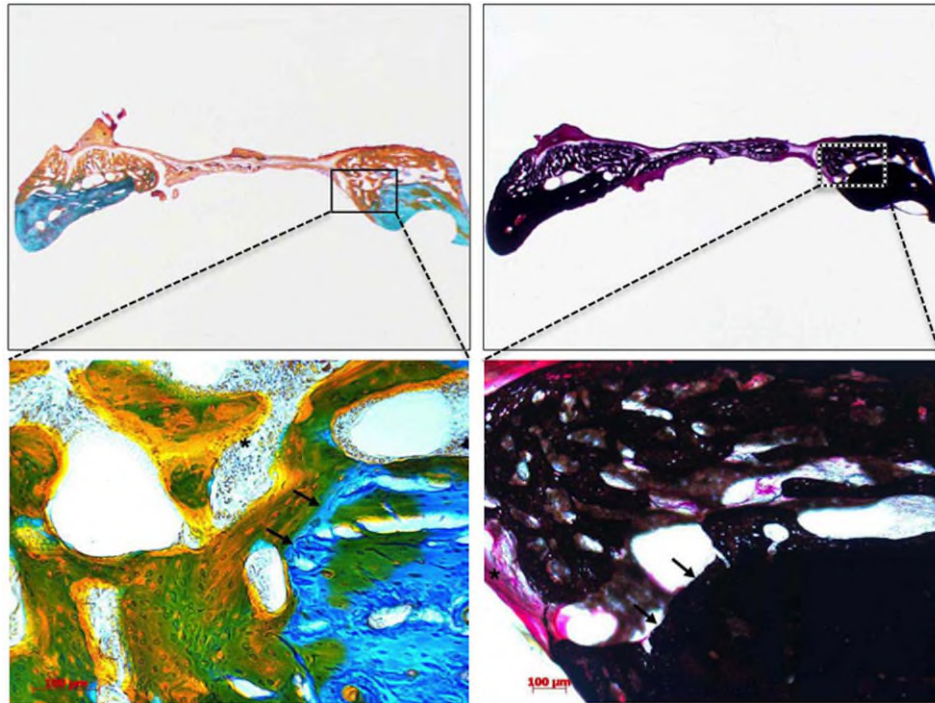


**FIGURE 6.** TMG (left) and vK staining (right) of woven bone ingrowth at day 28 in the 2.5 µg pBMP-2 group at the border with the original local bone (upper row; detail images are presented in the bottom row, with arrows indicating the transition zone between the NB and the original bone and with asterisks indicating the osteoid seam with numerous osteoblasts and adjacent connective tissue with fibroblasts). Magnification is  $\times 10$  in the top row,  $\times 200$  at the bottom left, and  $\times 100$  at the bottom right. Scale bar = 100 µm.

consolidation after 112 days (Fig. 7). In the higher-concentration plasmid groups with 50 and 100 µg pBMP-2, the former CSD was mostly filled with connective tissue. NB formation was visible only in the region adjacent to the edge of the mandibular CSD. The material that filled the rest of the CSD was still composed of cartilaginous cells and fibroblasts (Fig. 7).

Histological evidence further supported the  $\mu$ CT findings regarding the qualitative and quantitative evaluation of NB formation. The calculated NB volume was strongly correlated with the results obtained via  $\mu$ CT (Spearman's rank correlation coefficient  $r^2 = 0.91$ ,  $p < 0.001$ , Fig. 8).

#### Evaluation of bone dynamics via FL

Dynamic bone histomorphometric indices in the initial time of bone remodelling were evaluated via FL measurements and compared with the respective data for the control group, with native PDLA (Fig. 2). Because the share (%) of labelled NB ads up to 100% on day 27 in all groups this data are not shown. In the 2.5 µg pBMP-2 group, the portion of NB-formation at days 6 and 13 amounted to 26.9% of the total area of labelled NB, superior to those of the corresponding proportions in the therapy groups with 12.5 µg (22.3%), 25 µg (23.3%) as well as 50 and 100 µg pBMP-2 (Fig. 2). However, on day 6, the 2.5 µg pBMP-2 group also exhibited a higher percentage of calcification (14.7%) than the control group (6%), whereas by day 13, the calcification had increased to only 9.6% in the control group and had almost doubled in the 2.5 µg pBMP-2 group (30.7%). Nota-

bly, the percentage of calcification was considerably lower on day 6 in the 50 and 100 µg pBMP-2 groups than that in the 2.5 µg pBMP-2 group, and it remained approximately on the same low level as in the control group. With regard to all therapy groups statistically significant differences were observed in the 2.5 µg- and the 25 µg pBMP-2 group compared with the 50 pBMP-2 group on day 6 ( $p < 0.05$ ) and among the 12.5 µg pBMP-2 group and the 50 µg pBMP-2 group on day 13 ( $p < 0.05$ ). In contrast to the previous time points, on day 20, the cumulative dynamic NB formation in the 2.5 µg pBMP-2 group was even lower than that of all therapy groups (12.5, 25, 50, and 100 µg pBMP-2) but higher than that of the control (Fig. 2). Significance existed solely compared to the 50 µg pBMP-2 group ( $p < 0.05$ ). With regard to the PDLA control group the course and amount of FL were atypical as it differs significantly from the BV data in  $\mu$ CT at day 56 when NB was evident due to some extend of local GF expression because of the limited pH decrease within the first 50 days. This control group exhibited no significant difference in FL on day 6, but as expected there was significant less bone-inducing activity ( $p < 0.05$ ) on the measure points day 13 and 20 compared to all therapeutic groups (Fig. 2). But this NB was not sustained as visible in the course of FL completely different to that of the 2.5 µg plasmid group. As NB-formation into the defect was limited, in those groups, the four fluorochrome labels were in close proximity to each other especially at the outer edge of the defect in the latter groups. FL illustrated that the predominant fluorochrome labels were calcein blue and xylenol orange, which

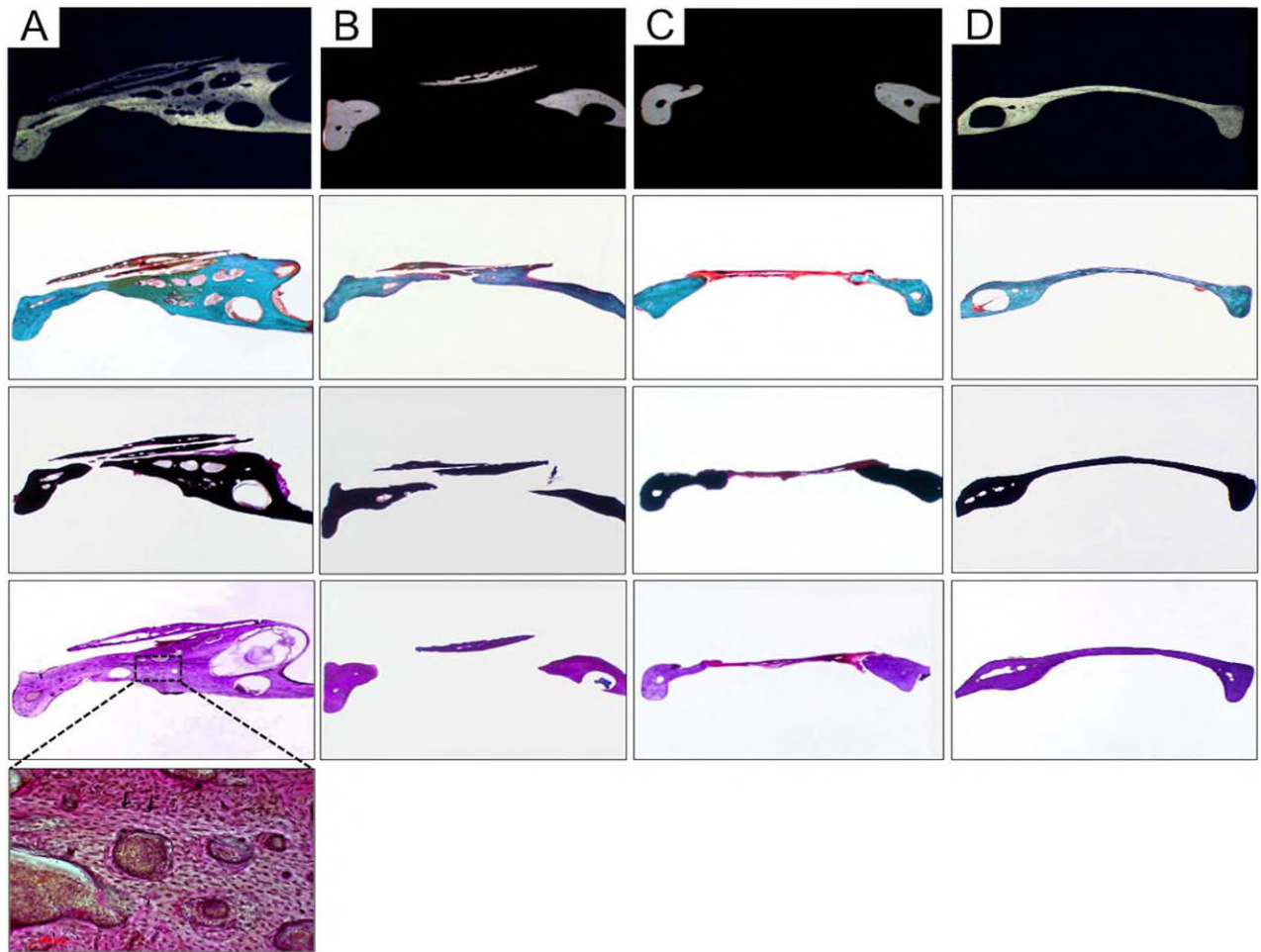


**FIGURE 7.** Histological study compared with microradiography of the same transverse view of the CSD at 112 days post-surgery for treatment with various pBMP-2 concentrations and PDLLA: 2.5 µg (column A), PDLLA (column B), 100 µg (column C), and a native untreated rat mandibular bone (column D). All images are presented at  $\times 10$  magnification except for the image at the bottom of column A, which is presented at  $\times 100$  and reveals well-organised, newly formed lamellar bone in the 2.5 µg group after 112 days (arrows). The asterisks indicate the osteoid trabeculae. All groups exhibited a certain amount of bone ingrowth, but the 2.5 µg pBMP-2 group demonstrated significantly more effective osteogenesis in the CSD area compared with PDLLA (column B) and the groups treated at higher concentrations, that is, the 100 µg group (column C). The rows contain microradiography images (1st row) and images corresponding to various stains: TMG (2nd row), vK (3rd row), and LL (4th row). Scale bar = 100 µm.

indicates that most of the bone turn over occurred within the first 14 days and continued up to the 27 days endpoint.

## DISCUSSION

Many advances to the effective use of regional GT for bone regeneration have been described; these approaches are generally either viral or nonviral and include either *ex vivo* or *in vivo* gene transfer. In the current study, a CSD model in rats, similar to that used in previous experiments, was used to demonstrate that NB formation with a shielded GAM to deliver the BMP-2 gene to the desired site to provide a period of sustained BMP production enables the effective and safe repair of the CSD area. The importance of a safe and stable delivery device has been demonstrated by previous studies using the same vector and plasmid technology for BMP-2 expression *in vitro*<sup>18</sup> and for fracture healing.<sup>42,43</sup> In one study, using a PDLLA coating similar to ours, it was possible to exclude any systemic spread of luciferase mRNA via rt-PCR of all parenchymatous organs and to

show local BMP-2 expression,<sup>42</sup> whereas in the other experiment, using the same vector technology but a metallic coating applied with fibrin glue instead of PDLLA, luciferase mRNA was detectable in almost all organs but without any efficient local osteoinductive effect due to the different mode of delivery.<sup>43</sup>

The lack of knowledge concerning the spatio-temporal characteristics of GT (an important issue) has never previously been addressed.<sup>44</sup> Therefore, one of the major goals of this study was to systematically evaluate the dose-dependent osteoinductive potential of the previously established GAM concept by incorporating the GV into the PDLLA coating to determine the optimal dose range that provided the maximum gene expression to the desired site for a certain period without inducing cell toxicity. Furthermore, the compatibility of a controlled delivery system with a stable metallic surface must be demonstrated. Instead of collagen, as used in previous experiments, titanium was chosen as the basic implant material because the latter is completely

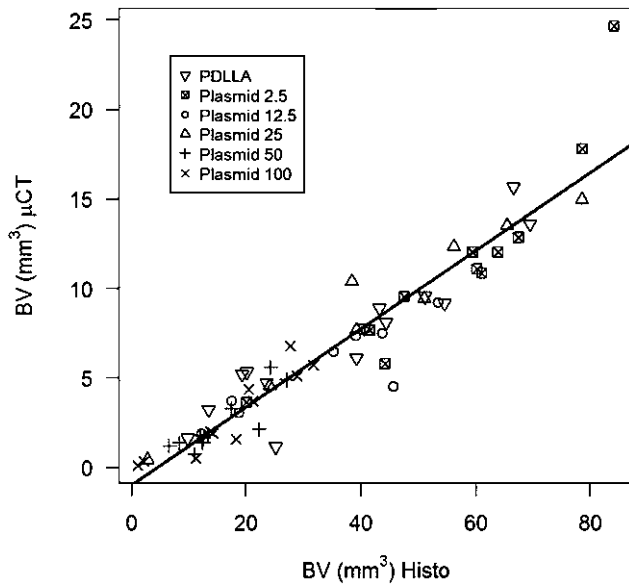


**FIGURE 8.** Correlation of 3D measurements obtained via  $\mu$ CT with histomorphometry ( $r^2 = 0.91$ ).

bio inert and easy to connect with the stable PDLLA coating. In various fields of bone surgery the use of coated titanium is common to boost osseointegration. Coated titanium osteosynthesis materials and joint replacement, are important medical fields for titanium surfaces. Further the osseointegration of dental implants could be sufficiently promoted by the use of coated titanium implants. Furthermore, we were looking for a delivery system that is transferable to human applications, for example, in dental implantology or CAD/CAM titanium implants.<sup>44</sup>

As established in previous analyses, various cell lines have been successfully transfected with a relatively high efficiency of up to 27%. In the current study, titanium foils coated with shielded pBMP-2 were tested in CSDs in rat mandibles. The effects of GFs are known to be dose-dependent.<sup>45,46</sup> However, data also exist indicating that GF can exert an inhibitory effect on bone regeneration, perhaps via osteoclastic stimulation.<sup>47,48</sup> As a consequence of the latter data, there is an urgent need for the dose dependency of this GAM to be further verified.<sup>48</sup> COPROGs that contain PEI are highly successful for gene delivery with a high transfection efficiency, but they also demonstrate relatively high cytotoxicity<sup>49</sup> that is affected by many factors, such as coating<sup>18,44</sup> particle size, molecular weight, ionic strength of the solution, degree of branching, and zeta potential.<sup>50</sup> In contrast to commercial high-molecular-weight materials, PEI, with its low molecular mass (10 kDa) and moderate branching, can achieve efficient delivery with low toxicity.<sup>51,52</sup> In our study, the high COPROG dosages in the 50 and 100  $\mu$ g pBMP-2 groups led to impaired bone regeneration (significantly lower than even that of the control group) and peri- and submandibular seromas at 10–14 days after implantation. This effect is most likely not directly associated with the amount of DNA but rather with the potential delayed toxicity of relatively high amounts PEI, a polycationic molecule that is a

component of the vector. Even though there will always be a dose-dependent toxicity of polycation-based DNA delivery systems, the toxicity of nanoparticles comprised of PEI and DNA can be limited by surface shielding.<sup>53,54</sup> In our previous work<sup>53</sup> and in this study we have used a non-covalent shielding strategy. Negatively charged protective copolymers are associated by electrostatic interaction with pre-formed positively charged PEI-DNA nanoparticles to result in COPROGs. Once these are released from the PDLLA coating and internalized in cells, the particles will dissociate and uncomplexed free PEI can exert its known toxic effects.<sup>55</sup> PEI can interact and aggregate with negatively charged cellular components, thus inhibiting normal cellular processes and leading to cell shrinkage, reduced occurrence of mitosis and vacuolisation of the cytoplasm. Hence, an approach of covalent PEG grafting to PEI or biodegradable PEI like described by Petersen et al. may be advantageous at high vector doses.<sup>54</sup>

Although intrinsic reparative cells can creep toward the implant, an effect that cannot be ruled out, little immature NB occurs at the defect margins, indicating that the intrinsic bone repair process is not sufficiently powerful in the case of CSDs, as observed in the native PDLLA group and in the control group of a previous experiment using uncoated titanium foils.<sup>23</sup> Regardless of whether NB formation is influenced by the recruitment of surrounding host cells, the results demonstrate the effective repair of CSD using a GAM within a certain therapeutic window. Biodegradable coating plays a pivotal role in bone tissue engineering.<sup>44</sup> In this study, the degradation of PDLLA may have occurred through both processes. The abundant circulation via the blood vessels initially formed in the defect area close to the surface of the implant can promote the hydrophilic dissolution process beginning after 4–5 days<sup>15,18</sup> and break the coating into small particles. Interestingly, control CSDs covered with native-PDLLA-coated implants exhibited substantial regeneration after 56 days mainly at the CSD edge, possibly due to a remodelling process initiated as a response to degradation of the PDLLA coating and the resulting pH decrease, as histologically observed from the local increase in lymphocytes and giant cells; however, after 112 days, the BV decreased significantly, indicating unsustainable NB formation. Our current data, which indicate an inverse COPROG-dose dependency and identify 2.5  $\mu$ g pBMP-2 as the most effective concentration, confirm previous *in vitro* results.<sup>15,18</sup> In this study, FL confirmed that the onset of NB occurred significantly more rapidly in the 2.5  $\mu$ g pBMP-2 group than in the other groups. In the initial phase, PDLLA implants loaded with 50  $\mu$ g and 100  $\mu$ g pBMP-2 even appeared to exert a suppressing influence on the initial calcification process. This effect flattened out as early as day 13 and was even similar on the later time points. This delay, that is probably due to a smaller amount of free unbound BMP-2 plasmid compared to the 2.5  $\mu$ g pBMP-2 group should not be underestimated when considering early osteoinduction for the accelerated osseointegration of implants when using GFs.

Recent studies have demonstrated that *ex vivo* transgene-activating cell transplantation with nonviral gene

transfer can effectively induce bone and cartilage regeneration in animal models. Although no clear-cut explanation exists for the favorable results obtained *in vivo* using less efficient nonviral gene transfer compared with viral vector systems, two factors seem to be important: First, the short-term transient expression of transgenes such as BMP by target cells continues for >1 week, although at low levels, as we have demonstrated previously *in vitro*.<sup>18</sup> This limited expression appears to be sufficient to induce successful bone repair in certain animal models. Second, the presence of BMP for only a few days might be important for recruiting a sufficient number of the required cells or initiating differentiation cascades. In our study, direct gene delivery via nonviral shielded vector technology efficiently introduced BMP-2 into cells that migrated into the defects during the initial bone healing. FL indicated that especially in the 2.5 µg group the high bone turnover primarily occurred in the initial phase no later than 14 days post surgery, as indicated by the relatively high levels of calcein blue and xylenol orange fluorescence. This is probably the effect of the paracrine stimulation of cells by the GAM concept within the first 14 days post surgery. This effect of initial bone promotion later resulted in the higher BV and the complete healing of the defect from day 56 to 112. Although *in vitro* transgene expression decreases after 1 week,<sup>18</sup> BMP production was maintained over 2 weeks, most likely because of the endogenous BMP released by nontransfected cells, which were most likely stimulated through a paracrine pathway, as demonstrated by the superior bone regeneration effect observed in the 2.5 µg group.

One difficulty encountered in direct gene delivery without *ex vivo* cell intervention is the inability to select and efficiently transfect target cells, as is possible under *in vitro* conditions. The direct application of non-viral vector systems in bone tissue engineering cannot ensure that a sufficient number of stem/progenitor cells are available at the place and time desired for gene delivery; this might be an important requirement for efficient tissue repair.<sup>56</sup> Therefore, we divided the 2.5 µg group into two groups based on the distance from the CSD to the root of the mandible incisor of the rat. The subgroup in which the CSD was adjacent to the incisor root exhibited significantly more NB formation than the subgroup in which there was no direct contact. This result provides a strong hint that the bone vessel supply and the migration of progenitor cells, which are more present in the region of the periodontal ligaments, have a significant influence on the efficacy of local GT.<sup>2,57</sup> The pattern of bone regeneration observed within the defects was also analyzed. This evaluation confirmed the finding that NB formation proceeded much more rapidly in the ventral regions of the CSDs.

Our results indicate that COPROGs carrying higher BMP-2 plasmid concentrations induce bone healing and osseointegration to a lesser degree in the centre of the CSD (centre ROI), compared with the complete healing observed in the other ROIs. This finding may also be attributable to the mobilisation of an insufficient number of target cells, for example, stem cells or osteogenic progenitors, to the centre

of the CSD at the time of direct gene delivery. Poor transfection efficiency may not be the cause of the incomplete healing observed in the central portion of the defect because most of the cells that migrated to the centre of the CSD were successfully transfected in our experiments. Furthermore, transfection efficiency should account for not only the number of cells transfected but also the amount of protein released. The amount of BMP-2 protein produced by each transfected cell may be an important factor in determining the potential for bone regeneration. The varying amounts of BMP-2 protein released from the transfected cells depending on the efficacy of the gene delivery system may also be responsible for the different capabilities of the transgene-activating cells to induce NB formation *in vivo*. Previous studies have suggested that coated metallic implants into which active ingredients have been incorporated could provide local drug release, thereby delivering a high drug concentration in the area of interest without systemic side effects. However, the use of an unstable coating on the metal surface, such as fibrin glue, may lead to an undesirable systemic spread of the vector without the desired local GT effect.<sup>43</sup>

## CONCLUSION

Our results suggest that a metallic surface coated with PDLLA and a protected plasmid can provide a morphogenetic signal that can address the problem of spatio-temporal gene control. Such a construct exerts a synergistic effect to promote rapid bone formation. The described approach may provide a new therapeutic modality for GT in the case of bony CSDs. Investigations of various types of bone healing in large animal models using combined therapies involving both cells and various vector and promoter systems will be necessary to determine future applications.

## ACKNOWLEDGMENTS

The authors thank Professor Kunzelmann, Department of Restorative Dentistry, LMU-University, Munich, Germany, for commercial providing the µCT 40.

## REFERENCES

1. Smeets R, Barbeck M, Hanken H, Fischer H, Lindner M, Heiland M, Wöltje M, Ghanaati S, Kolk A. Selective laser-melted fully biodegradable scaffold composed of poly(D,L-lactide) and β-tricalcium phosphate with potential as a biodegradable implant for complex maxillofacial reconstruction: In vitro and in vivo results. *J Biomed Mater Res B Appl Biomater* 2016 Apr 8. doi: 10.1002/jbm.b.33660. [Epub ahead of print]
2. Fischer J, Kolk A, Wolfart S, Pautke C, Warnke PH, Plank C, Smeets R. Future of local bone regeneration—Protein versus gene therapy. *J Craniomaxillofac Surg* 2011;39:54–64.
3. Langer R, Vacanti JP. Tissue engineering. *Science* 1993;260:920–926.
4. Kolk A, Handschel J, Drescher W, Rothamel D, Kloss F, Blessmann M, Heiland M, Wolff KD, Smeets R. Current trends and future perspectives of bone substitute materials—From space holders to innovative biomaterials. *J Craniomaxillofac Surg* 2012; 40:706–718.
5. Smeets R, Maciejewski O, Gerressen M, Spiekermann H, Hanisch O, Riediger D, Blake F, Stein J, Holzle F, Kolk A. Impact of rhBMP-2 on regeneration of buccal alveolar defects during the

- osseointegration of transgingival inserted implants. *Oral Surg Oral Med Oral Pathol Oral Radiol Endod* 2009;108:e3–e12.
6. Cowan CM, Jiang X, Hsu T, Soo C, Zhang B, Wang JZ, Kuroda S, Wu B, Zhang Z, Zhang X, Ting K. Synergistic effects of Nell-1 and BMP-2 on the osteogenic differentiation of myoblasts. *J Bone Miner Res* 2007;22:918–930.
  7. Ehnert S, Zhao J, Pscherer S, Freude T, Dooley S, Kolk A, Stockle U, Nussler AK, Hube R. Transforming growth factor beta1 inhibits bone morphogenic protein (BMP)-2 and BMP-7 signaling via upregulation of Ski-related novel protein N (SnoN): Possible mechanism for the failure of BMP therapy? *BMC Med* 2012;10: 101.
  8. Schillinger U, Wexel G, Hacker C, Kullmer M, Koch C, Gerg M, Vogt S, Ueblacker P, Tischer T, Hensler D, et al. A fibrin glue composition as carrier for nucleic acid vectors. *Pharm Res* 2008;25: 2946–2962.
  9. Vogt S, Wexel G, Tischer T, Schillinger U, Ueblacker P, Wagner B, Hensler D, Wilisch J, Geis C, Wubbenhorst D, et al. The influence of the stable expression of BMP2 in fibrin clots on the remodeling and repair of osteochondral defects. *Biomaterials* 2009;30: 2385–2392.
  10. Ueblacker P, Wagner B, Vogt S, Salzmann G, Wexel G, Kruger A, Plank C, Brill T, Specht K, Hennig T, et al. In vivo analysis of retroviral gene transfer to chondrocytes within collagen scaffolds for the treatment of osteochondral defects. *Biomaterials* 2007;28: 4480–4487.
  11. Scheller EL, Krebsbach PH. Gene therapy: Design and prospects for craniofacial regeneration. *J Dent Res* 2009;88:585–596.
  12. Elangovan S, D'Mello SR, Hong L, Ross RD, Allamargot C, Dawson DV, Stanford CM, Johnson GK, Sumner DR, Salem AK. The enhancement of bone regeneration by gene activated matrix encoding for platelet derived growth factor. *Biomaterials* 2013;35: 737–747.
  13. Evans CH, Huard J. Gene therapy approaches to regenerating the musculoskeletal system. *Nat Rev Rheumatol* 2015;11:234–242.
  14. De Laporte L, Shea LD. Matrices and scaffolds for DNA delivery in tissue engineering. *Adv Drug Deliv Rev* 2007;59:292–307.
  15. Reckhenrich AK, Koch C, Egana JT, Plank C. The use of non-viral gene vectors for bioactive poly-(D, L-lactide) implant surfaces in bone tissue engineering. *Eur Cell Mater* 2012;23:441–448.
  16. Rafat M, Cleroux CA, Fong WG, Baker AN, Leonard BC, O'Connor MD, Tsilfidis C. PEG-PLA microparticles for encapsulation and delivery of Tat-EGFP to retinal cells. *Biomaterials* 2010;31:3414–3421.
  17. Smeets R, Gerhards F, Stein J, Paz RM, Vogt S, Pautke C, Weitz J, Kolk A. A novel hemostatic delivery device for thrombin: Biodegradable poly(D, L-lactide-co-glycolide) 50:50 microspheres. *J Biomed Mater Res A* 2011;96:177–185.
  18. Kolk A, Haczek C, Koch C, Vogt S, Kullmer M, Pautke C, Deppe H, Plank C. A strategy to establish a gene-activated matrix on titanium using gene vectors protected in a polylactide coating. *Biomaterials* 2011;32:6850–6859.
  19. Bessa PC, Casal M, Reis RL. Bone morphogenetic proteins in tissue engineering: The road from laboratory to clinic, part II (BMP delivery). *J Tissue Eng Regen Med* 2008;2:81–96.
  20. Kanakaris NK, Calori GM, Verdonk R, Burssens P, De Biase P, Capanna R, Vangosa LB, Cherubino P, Baldo F, Ristinieni J, et al. Application of BMP-7 to tibial non-unions: A 3-year multicenter experience. *Injury* 2008;39:S83–S90.
  21. Finsinger D, Remy JS, Erbacher P, Koch C, Plank C. Protective copolymers for nonviral gene vectors: Synthesis, vector characterization and application in gene delivery. *Gene Ther* 2000;7:1183–1192.
  22. Honig D, DeRouchev J, Jungmann R, Koch C, Plank C, Radler JO. Biophysical characterization of copolymer-protected gene vectors. *Biomacromolecules* 2010;11:1802–1809.
  23. Deppe H, Stemberger A, Hillemanns M. Effects of osteopromotive and anti-infective membranes on bone regeneration: An experimental study in rat mandibular defects. *Int J Oral Maxillofac Implants* 2003;18:369–376.
  24. Parrilla C, Lattanzi W, Rita Fetoni A, Bussu F, Pola E, Paludetti G. Ex vivo gene therapy using autologous dermal fibroblasts expressing hLMP3 for rat mandibular bone regeneration. *Head Neck* 2010;32:310–318.
  25. Schliephake H, Weich HA, Dullin C, Gruber R, Frahse S. Mandibular bone repair by implantation of rhBMP-2 in a slow release carrier of polylactic acid—An experimental study in rats. *Biomaterials* 2008;29:103–110.
  26. Morgan EF, Mason ZD, Chien KB, Pfeiffer AJ, Barnes GL, Einhorn TA, Gerstenfeld LC. Micro-computed tomography assessment of fracture healing: Relationships among callus structure, composition, and mechanical function. *Bone* 2009;44:335–344.
  27. Ruegsegger P, Koller B, Muller R. A microtomographic system for the nondestructive evaluation of bone architecture. *Calcif Tissue Int* 1996;58:24–29.
  28. Nazarian A, Snyder BD, Zurakowski D, Muller R. Quantitative micro-computed tomography: A non-invasive method to assess equivalent bone mineral density. *Bone* 2008;43:302–311.
  29. Barbier A, Martel C, de Vernejoul MC, Tirode F, Nys M, Mocaer G, Morieux C, Murakami H, Lacheretz F. The visualization and evaluation of bone architecture in the rat using three-dimensional X-ray microcomputed tomography. *J Bone Miner Metab* 1999;17: 37–44.
  30. Muller R, Van Campenhout H, Van Damme B, Van Der Perre G, Dequeker J, Hildebrand T, Ruegsegger P. Morphometric analysis of human bone biopsies: A quantitative structural comparison of histological sections and micro-computed tomography. *Bone* 1998;23:59–66.
  31. Donath K, Breuner G. A method for the study of undecalcified bones and teeth with attached soft tissues. The Sage-Schliff (sawing and grinding) technique. *J Oral Pathol* 1982;11:318–326.
  32. Laczko J, Levai G. Simple differential staining method for semithin sections of ossifying cartilage and bone tissues embedded in epoxy-resin. *Mikroskopie* 1975;31:1–4.
  33. Parfitt AM, Drezner MK, Glorieux FH, Kanis JA, Malluche H, Meunier PJ, Ott SM, Recker RR. Bone histomorphometry: Standardization of nomenclature, symbols, and units. Report of the ASBMR Histomorphometry Nomenclature Committee. *J Bone Miner Res* 1987;2:595–610.
  34. Jenö L, Geza L. A simple differential staining method for semithin sections of ossifying cartilage and bone tissues embedded in epoxy resin. *Mikroskopie* 1975;31:1–4.
  35. Fritsch H. Staining of different tissues in thick epoxy resin-impregnated sections of human fetuses. *Stain Technol* 1989;64: 75–79.
  36. Gruber HE. Adaptations of Goldner's Masson trichrome stain for the study of undecalcified plastic embedded bone. *Biotech Histochem* 1992;67:30–34.
  37. Hahn M, Vogel M, Pompesius-Kempa M, Delling G. Trabecular bone pattern factor—A new parameter for simple quantification of bone microarchitecture. *Bone* 1992;13:327–330.
  38. Rahn BA, Perren SM. Alizarin complexon-fluorochrome for bone and dentine labeling. *Experientia* 1972;28:180.
  39. Rahn BV, Bacellar FC, Trapp L, Perren SM. A method for morphometry of bone formation using fluorochromes (author's transl). *Aktuelle Traumatol* 1980;10:109–115.
  40. Pautke C, Tischer T, Vogt S, Haczek C, Deppe H, Neff A, Horch HH, Schieker M, Kolk A. New advances in fluorochrome sequential labelling of teeth using seven different fluorochromes and spectral image analysis. *J Anat* 2007;210:117–121.
  41. Pautke C, Vogt S, Tischer T, Wexel G, Deppe H, Milz S, Schieker M, Kolk A. Polychrome labeling of bone with seven different fluorochromes: Enhancing fluorochrome discrimination by spectral image analysis. *Bone* 2005;37:441–445.
  42. Schwabe P, Greiner S, Ganzert R, Eberhart J, Dahn K, Stemberger A, Plank C, Schmidmaier G, Wildemann B. Effect of a novel non-viral gene delivery of BMP-2 on bone healing. *Sci World J* 2012; 2012:560142.
  43. Faensen B, Wildemann B, Hain C, Hohne J, Funke Y, Plank C, Stemberger A, Schmidmaier G. Local application of BMP-2 specific plasmids in fibrin glue does not promote implant fixation. *BMC Musculoskelet Disord* 2011;12:163.
  44. Gotz C, Warnke PH, Kolk A. Current and future options of regeneration methods and reconstructive surgery of the facial skeleton. *Oral Surg Oral Med Oral Pathol Oral Radiol* 2015;120:315–323.

45. Meinel L, Zoidis E, Zapf J, Hassa P, Hottiger MO, Auer JA, Schneider R, Gander B, Luginbuehl V, Bettschart-Wolfisberger R, et al. Localized insulin-like growth factor I delivery to enhance new bone formation. *Bone* 2003;33:660–672.
46. Terheyden H, Menzel C, Wang H, Springer IN, Rueger DR, Acil Y. Prefabrication of vascularized bone grafts using recombinant human osteogenic protein-1—Part 3: Dosage of rhOP-1, the use of external and internal scaffolds. *Int J Oral Maxillofac Surg* 2004;33:164–172.
47. Okamoto M, Murai J, Yoshikawa H, Tsumaki N. Bone morphogenetic proteins in bone stimulate osteoclasts and osteoblasts during bone development. *J Bone Miner Res* 2006;21:1022–1033.
48. Rose L, Uludag H. Realizing the potential of gene-based molecular therapies in bone repair. *J Bone Miner Res* 2013;28:2245–2262.
49. Kim YH, Park JH, Lee M, Park TG, Kim SW. Polyethylenimine with acid-labile linkages as a biodegradable gene carrier. *J Control Release* 2005;103:209–219.
50. Kunath K, von Harpe A, Fischer D, Petersen H, Bickel U, Voigt K, Kissel T. Low-molecular-weight polyethylenimine as a non-viral vector for DNA delivery: Comparison of physicochemical properties, transfection efficiency and in vivo distribution with high-molecular-weight polyethylenimine. *J Control Release* 2003; 89:113–125.
51. Fischer D, Bieber T, Li Y, Elsasser HP, Kissel T. A novel non-viral vector for DNA delivery based on low molecular weight, branched polyethylenimine: Effect of molecular weight on transfection efficiency and cytotoxicity. *Pharm Res* 1999;16:1273–1279.
52. Godbey WT, Wu KK, Mikos AG. Size matters: Molecular weight affects the efficiency of poly(ethylenimine) as a gene delivery vehicle. *J Biomed Mater Res* 1999;45:268–275.
53. Scherer F, Schillinger U, Putz U, Stemberger A, Plank C. Nonviral vector loaded collagen sponges for sustained gene delivery in vitro and in vivo. *J Gene Med* 2002;4:634–643.
54. Petersen H, Fechner PM, Martin AL, Kunath K, Stolnik S, Roberts CJ, Fischer D, Davies MC, Kissel T. Polyethylenimine-graft-poly(ethylene glycol) copolymers: Influence of copolymer block structure on DNA complexation and biological activities as gene delivery system. *Bioconjug Chem* 2002;13:845–854.
55. Godbey WT, Wu KK, Mikos AG. Poly(ethylenimine)-mediated gene delivery affects endothelial cell function and viability. *Biomaterials* 2001;22:471–480.
56. Evans CH. Gene delivery to bone. *Adv Drug Deliv Rev* 2012;64: 1331–1340.
57. Park J, Lutz R, Felszeghy E, Wiltfang J, Nkenke E, Neukam FW, Schlegel KA. The effect on bone regeneration of a liposomal vector to deliver BMP-2 gene to bone grafts in peri-implant bone defects. *Biomaterials* 2007;28:2772–2782.